Advanced Synthesis & Catalysis

ADVANCED SYNTHESIS & CATALYSIS
advsynthcatal.com

RESEARCH ARTICLE OPEN ACCESS

Catalytic Enantioselective Synthesis of Conformationally Stable C(sp^2)–C(sp^3) Naphthocoumarin Atropisomers

M. Chiara Cabua[1] | Davide Moi[1,2] | Emanuele Cocco[1,3] | Valentina Onnis[2] | Enrico Podda[1] | David J. Aitken[4] | Armando Carlone[3] | Renzo Luisi[5] | Enrica Tuveri[1] | Drew F. Parsons[1] | Francesco Secci[1]

[1]Dipartimento di Scienze Chimiche e Geologiche, Università degli Studi di Cagliari, Cagliari, Italy | [2]Dipartimento di Scienze della Vita e dell'Ambiente, Università degli Studi di Cagliari, Cagliari, Italy | [3]Department of Physical and Chemical Sciences, Consorzio C.I.N.M.P.I.S., Università degli Studi dell'Aquila, L'Aquila, Italy | [4]Université Paris-Saclay CNRS, ICMMO, Université Paris-Saclay, Orsay, France | [5]Department of Pharmacy-Drug Sciences, FLAME-Lab, Flow Chemistry and Microreactor Technology Laboratory, Università degli Studi di Bari (Aldo Moro), Bari, Italy

Correspondence: Davide Moi (dmoi@unica.it) | Francesco Secci (fsecci@unica.it)

Received: 19 February 2026 | **Revised:** 19 March 2026 | **Accepted:** 22 March 2026

Keywords: atropisomers | coumarin | enantioselective synthesis | naphthoquinone | organocatalysis

ABSTRACT

A straightforward atroposelective access to enantiomerically enriched 2-hydroxy-3-(2-oxochroman-4-yi)naphthalene-1,4-diones (with yields ranging from 32% to 87% and enantiomeric excesses up to 99%) is described. Using an organocatalytic approach, 2-hydroxynaphthoquinone reacts with a 3-coumarin-3-carboxylic acid through a tandem 1,4-addition/decarboxylation process initiated by a thiourea-functionalized cinchona alkaloid, which efficiently controls the stereochemistry of a newly forged stereocenter, while simultaneously directing the formation of a configurationally stable C(sp^2)–C(sp^3) synclinal atropisomer. The methodology has been explored across a broad substrate scope, and the results are supported by detailed nuclear magnetic resonance (NMR) analyses, single-crystal X-ray diffraction, and density functional theory (DFT) calculations.

1 | Introduction

The synthesis of C(sp^2)–C(sp^3) atropisomers is a process that is finely controlled by steric factors that prevent the free rotation of two domains of a molecule around a stereogenic axis [1, 2]. Numerous procedures related to the preparation of C(sp^2)-C(sp^2) atropisomers are reported in the literature, with particular reference to the synthesis of biaryl [3] and C(sp^2)-heteroaromatic compounds [4–7], which have been extensively studied by many authors. Other atropoisomeric molecular architectures, such as amides and imides, characterized by the presence of a configurationally stable stereogenic axis, have also been described [8–11]. These studies have prompted the development of different synthetic approaches, including organocatalysis [12], biocatalysis [13–16], and organometallic-based strategies [17–19]. In contrast, there are relatively few reports concerning the identification of efficient synthetic methodologies capable of generating molecular species with a high rotational stability of the stereogenic axis ($\Delta G_{rot} > 125$ kJ/mol), resistant to epimerization along a C(sp^2)–C(sp^3) single bond. This is a challenge that becomes increasingly difficult to meet due to the flexibility of such structures that plays a crucial role in their three-dimensional organization [20–22] (Scheme 1c). In fact, the greater rotational freedom of C(sp^2)–C(sp^3) bonds allows such structures to spatially reorganize, significantly affecting the impact of steric factors as well as the stabilizing contribution of intra and intermolecular forces, such as hydrogen bonding, which in some cases provides the configurational stability in biaryl systems [23]. In 2019, Bertuzzi, Corti, and coworkers reported a series of studies dealing with the synthesis of C(sp^2)–C(sp^3) derivatives endowed with axial chirality using an organocatalytic approach [24]. This exploited asymmetric induction using chiral phosphoric acids (CPA) to achieve central-to-axial chirality conversion via a Povarov cycloaddition reaction and enabled the enantioselective synthesis of configurationally stable indole-quinoline atropisomers. Moreover, Bencivenni developed an enantioselective

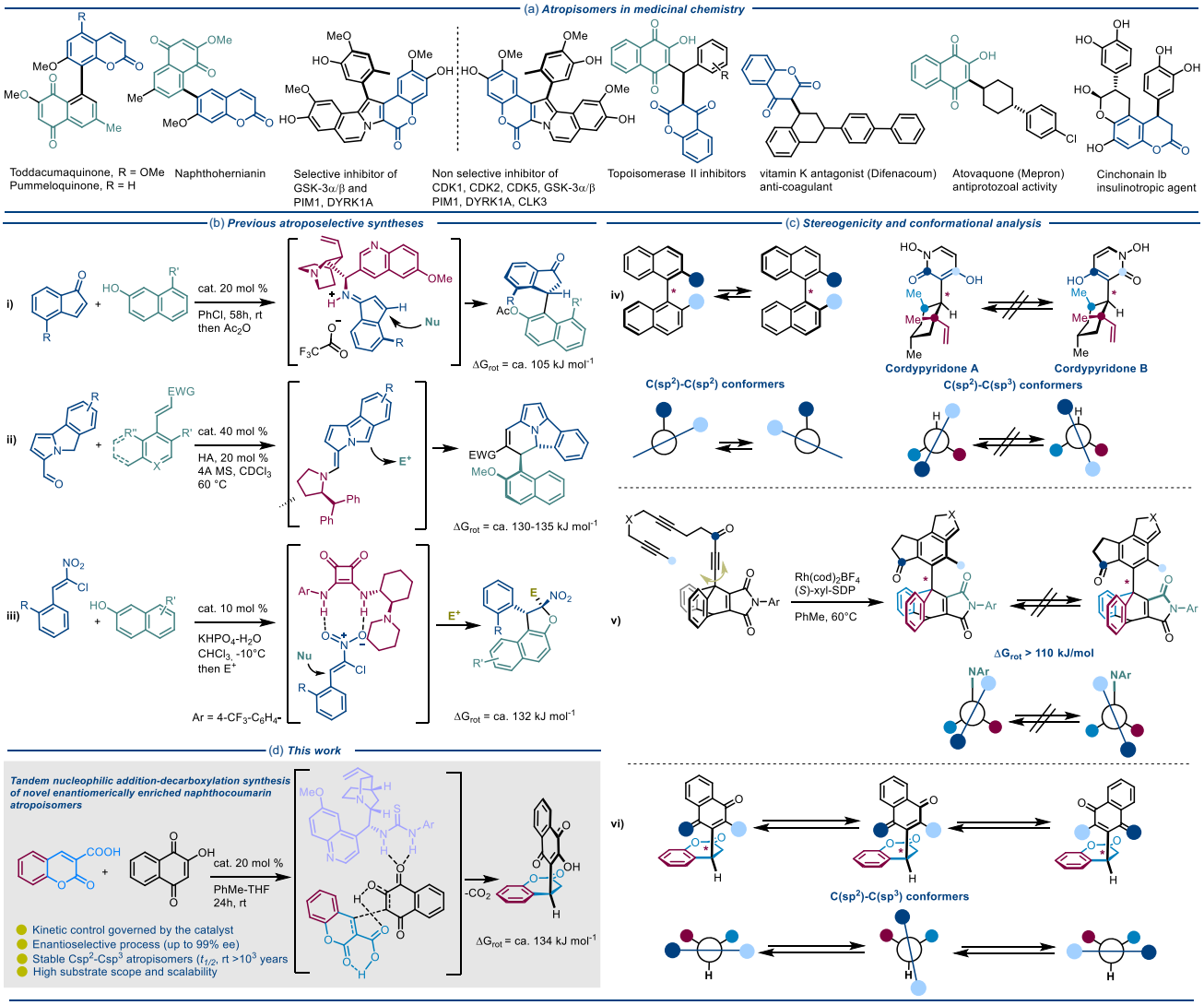

SCHEME 1 | Natural and synthetic bioactive compounds featuring stereogenic axes. (a) Examples of biologically active compounds featuring chromanones possessing C(sp^2)-C(sp^2) and C(sp^2)–C(sp^3) stereogenic axes. (b) Previously reported atroposelective preparations of C(sp^2)–C(sp^3) compounds. (c) Stereogenicity and conformational analysis. Prototypical biaryl atropisomers characterized by elevated bond-rotational barriers and typical rotational barriers of C(sp^2)–C(sp^3) derivatives. (d) Our approach to access enantiomerically enriched C(sp^2)–C(sp^3) naphthocoumarin atropisomers.

Friedel–Crafts-type alkylation of β-naphthols with inden-1-ones, which allowed partial control of C(sp^2)–C(sp^3) axial conformers through asymmetric induction and reaction pathway control using cinchona alkaloids as catalysts (Scheme 1b,i). These discoveries represent seminal example in this field [25].

More recently, Jørgensen reported the construction of nonbiaryl, conformationally stable C(sp^2)–C(sp^3) atropisomers via a chiral amine-catalyzed cycloaddition reaction between 5H-benzo[a]pyrrolizine-3-carbaldehydes and nitroolefins (Scheme 1b,ii), affording the desired cyclo[3.2.2]azines with a high degree of control over the stereogenic axis [26]. Both of these synthetic strategies rely on organocatalytic approaches via covalent bonding iminium-enamine catalysis [27, 28]. Concurrently with the drafting of this work, Bao, Bonne, and colleagues reported a new atroposelective synthesis of 3-aryl-benzofurans (Scheme 1b,iii) using chiral squaramides as catalysts, capable of promoting the enantioselective addition of β-naphthols to nitro-Michael adducts with excellent results [29]. A distinct case, compared with those previously discussed, is the elegant study reported by Sparr and coworkers, in which a rhodium-catalyzed [2 + 2 + 2] cyclotrimerization governs the formation of one out of six possible stereoisomers featuring restricted rotation about a C(sp^2)–C(sp^3) axis. These interlocked structures give rise to configurationally stable atropisomers with six pronounced rotational barriers [2] (Scheme 1c). It is therefore evident that this research area, beyond the aforementioned studies, remains largely unexplored despite the significant biological and pharmaceutical importance of compounds possessing stereogenic axes. Moreover, a considerable amount of work is still required to establish novel synthetic strategies that provide access to both building blocks and bioactive molecules (Scheme 1a) with these intricate structural characteristics [30–33]. Addressing the aforementioned challenges, we report herein an innovative atroposelective tandem nucleophilic addition/decarboxylation reaction of 2-hydroxynaphthoquinones with coumarin-3-carboxylic acid derivatives [34–36], allowing access to a new class of conformationally stable 2-hydroxy-3-(2-oxochroman-4-yl)naphthalene-1,4-diones exhibiting C(sp^2)–C(sp^3)

atropisomers under kinetic control (Scheme 1d). 1,4-Addition/decarboxylation reactions [37, 38] of coumarin carboxylic acids have been previously studied using different nucleophiles, including indoles [39], cyclic 1,3-diketones [40], *N*-methylmorpholine [41], or 2-methylpyridine derivatives [42]. However, to the best of our knowledge, only one example of enantioselective tandem conjugate-addition/decarboxylation reaction of coumarin-3-carboxylic acids has been reported to date in the literature. This was described by Nakamura in 2016 and was employed to install a methyl-sulphonyl unit at position 4 of a chromenone core [43].. In our proposed approach, the reaction proceeds through the formation of hydrogen bonds between a thiourea-based cinchona alkaloid catalyst (**CT1**), which directs the 1,4-addition of naphthoquinones **2** to coumarin-3-carboxylic acids **1**. The generation of a stereocenter at the 4-position of the chromenone is accompanied by a decarboxylation process, resulting in the formation of substituted 2-hydroxy-3-(2-oxochroman-4-yl)naphthalene-1,4-diones **3**, characterized by a high degree of control over a $C(sp^2)–C(sp^3)$ axis. This achievement represents the first access to conformationally stable atropisomeric oxo-chromane naphthalenes *via* an enantioselective organocatalytic strategy. Furthermore, this procedure provides a new synthetic route to atropoisomeric hybrid coumarin-naphthoquinone structures; such compounds are known for their diverse and pronounced biological activities [44–49], as well as serving as indispensable tools in the design of new therapeutic agents [50].

2 | Results and Discussion

Initially, we evaluated a range of catalysts capable of promoting the reaction between coumarin **1a** and 2-hydroxynaphthoquinone **2a** (Scheme 2). Preliminary studies revealed that reactions carried out at room temperature in the presence of catalytic amounts of cinchona-based catalysts (20 mol %) led to the formation of the desired product **3aa** in good chemical yields using THF or DMF as solvents (See SI, Section S2). However, the enantiomeric excesses (*ee*) observed were negligible. Further optimization of the reaction conditions demonstrated that using toluene as a solvent in combination with the cinchona-derived thiourea catalyst **CT1**-(*R*), (20 mol %) enabled access to compound **3aa** with an isolated yield of about 38% and an *ee* of 98% after 72 h at rt, suggesting poor catalytic turnover (Scheme 2a). At this point, we conducted a series of experiments to determine whether the thiourea catalyst was decomposing during the reaction or whether it exhibited a higher binding affinity for the reaction product **3aa** than for the 2-hydroxynaphthoquinone **2a**. After confirming the catalyst's stability even after 80 h of

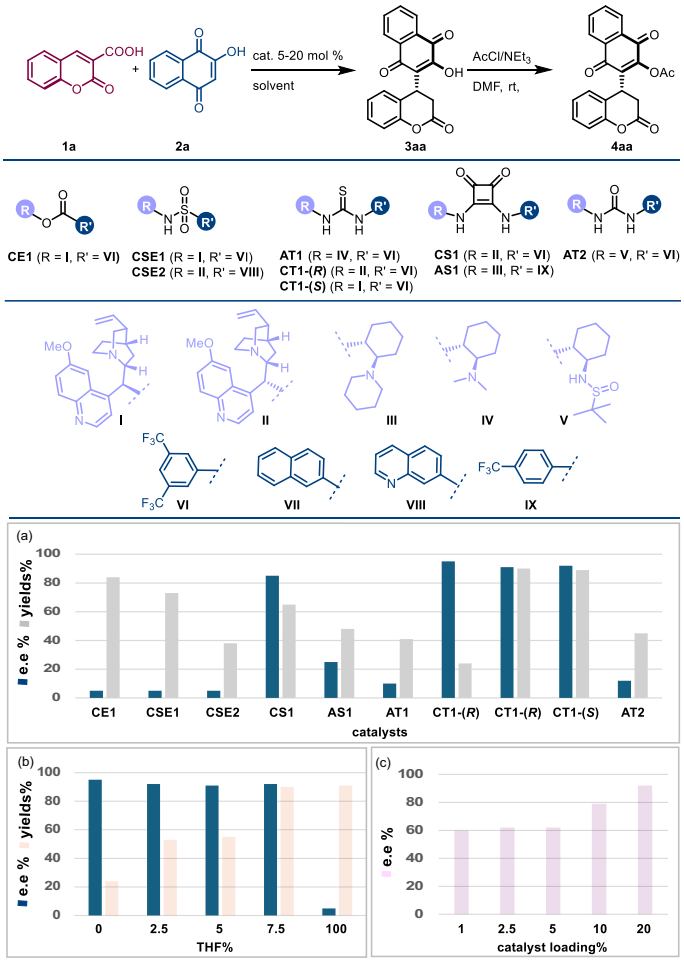

SCHEME 2 | Optimization of reaction conditions. (a). Catalyst screening; refer to Supporting Information for solvents (Table S1). (b) Effect of THF (equiv.) on chemical yields and enantiomeric excess (ee, Table S2). (c) Catalyst loading optimization (Table S3).

reaction, we performed nuclear magnetic resonance (NMR) titration experiments to measure the association constants (K_{ass}) between the nucleophile and the catalyst and between the catalyst and the reaction product (SI, Section S2.3), considering 1:1 interactions [51–53]. These binding studies demonstrate that **CT1** engages in significant noncovalent interactions with substrate **2a** ($K_{ass} = 2.90 \times 10^2\ M^{-1}$), primarily through hydrogen bonding between the thiourea moiety and a carbonyl group of the naphthoquinone framework (SI, Figures S7, S8 and Table S7). On the other hand, **CT1** exhibits a markedly higher association constant with product **3aa** ($K_{ass} = 1.03 \times 10^4\ M^{-1}$), representing a 35-fold increase in affinity (SI, Figures S9, S10, and Table S8). This pronounced preference for association with the reaction product strongly supports the hypothesis that once formed, **3aa** sequesters the catalyst, thereby preventing its participation in subsequent catalytic cycles and ultimately limiting turnover efficiency (SI, Figure S11). We therefore explored the addition of small amounts of THF to the reaction medium (Scheme 2b), reasoning that its role as a hydrogen-bond acceptor (or, if preferred, as a hydrogen-bond-breaking agent) might displace the bound naphthocoumarin product **3aa**, thereby regenerating the active catalyst (SI, Figure S12) [54–56]. Indeed, by adding 9.0 equiv. of THF, the isolated yield increased from 38% to over 85%, while maintaining comparable enantiomeric excess values after 24 h of reaction. In line with this result, reactions were carried out using the opposite enantiomer of the catalyst (**CT1**-(*S*)), which led to the formation of the corresponding epimer **3aa'** with an isolated yield of 83% and 94% *ee*.

Prompted by these encouraging observations, we carried out further studies aimed at reducing the catalyst loading. While good results were obtained in terms of chemical yields, we observed a systematic erosion of *ee* values at loadings below 20% (Scheme 2c). Indeed, it was observed that there is a significant uncatalyzed reaction that competes with the stereoselective process, therefore compromising the enantiomeric excess (see Supporting Information, Table S1). We therefore continued our research using toluene-THF (9.0 equiv.) as the reaction solvent and employing a 20% loading of **CT1**-(*R*). On the other hand, the reaction was easily scaled up to 2 g using coumarin **1a**, maintaining both the enantiomeric excess and the chemical yields undiminished. At this point, we extended the application of the described protocol to other 3-carboxycoumarin derivatives (**1b**-**1u**), keeping the naphthoquinone **2a** unchanged (Scheme 3a). Under the optimized reaction conditions, we obtained a variety of naphthocoumarin compounds **3ba**-**3ua** with chemical yields ranging from 41% to 85% and good to excellent *ee* (60% to > 99%), demonstrating broad applicability and high functional group tolerance. In fact, substituents at positions 6 and 7 on the coumarin scaffold, including halogens (F, Cl, Br), alkyl and alkoxy groups, nitro groups, and aryl moieties, were well tolerated. In contrast, substitution at position 8 led to good chemical yields but a significant drop in enantioselectivity, except for the disubstituted 6,8-diiodo compound **3qa** (92% *ee*). The absolute configuration of compound **3qa** was determined by single-crystal X-ray diffraction analysis of the corresponding acylated derivative **4qa** and found to be (*R*). This configuration was then assigned by analogy to the entire series and further supported by comparison between calculated and experimental electronic circular dichroism (ECD) measurements (see Supporting Information – Section S9). We subsequently expanded the scope of this transformation by employing a series of substituted naphthoquinone derivatives (**2b**-**j**), bearing diverse functional groups and exhibiting progressively increasing steric demand as well as electronic variations (Scheme 3b). These were reacted with a range of differently substituted coumarin carboxylic acids to assess potential steric and electronic effects that could impact the general applicability of the transformation. The presence of aliphatic, aryl, halogen, or methoxy groups did not significantly affect the overall performances, and the corresponding naphthocoumarin adducts **3db**-**3dh**, **3dj**, **3cg**, and **3ai** were isolated in good chemical yields. However, it was observed that varying the substituent on the naphthoquinone derivatives impacted the enantioselection. The measured *ee* values ranged from 71% for the brominated compound **3db** to 88% for the fluorinated derivative **3dd** at the same position and an intermediate value for the chlorinated adduct **3dc** (84%). This might suggest an impact of the electronic properties imparted to the naphthoquinone and its relationship with the catalyst or, again, a size effect, which is also discussed further in this study.

Similarly, the effect of electron-donating groups, as seen in compounds **3de**-**3dg**, appeared to be beneficial, leading to an increase in *ee* values that varied from 80% to 94% depending on the substituent (Me or OMe) and its position. Finally, the use of more sterically hindered naphthoquinones (**3dh**, **3ai,** and **3dj**) yielded the corresponding derivatives with variable enantiomeric excesses, as illustrated in the final part of Scheme 3b. To rationalize these results, we constructed Hammett plots correlating the *e.r.* (Log KM/Km, with M: major enantiomer and m: minor enantiomer) with the substituent constants (σ) attributable to the groups functionalizing both compounds **1** and **2** [57]. For 7-substituted coumarins **1**, a clear linear increase trend was observed when going from strongly electron-donating groups (e.g., **3ha**, OMe) to substituents that provide weaker stabilization of the α,β-unsaturated system, impacting the *ee*. Conversely, the absence of substituents (e.g., **3aa**, R = H) or the presence of electron-withdrawing groups (e.g., **3ba**, F; **3ca**, Cl) favor higher selectivity, consistently delivering *ee* values > 93%.

Extending the same type of analysis to 6-substituted coumarins **1** and 7-substituted naphthoquinones **2**, no decisive correlation was observed (see Supporting Information – Section 2 for details). As with the previous series, the absolute configuration of product **3df** was confirmed by single-crystal X-ray analysis of its acylated derivative **4df** (Scheme 3c) and determined to be (*R*). At this point, we assessed the configurational stability of the newly formed stereocenter by treating the enantiomerically enriched compounds **3aa** and **3da** with an excess of triethylamine for extended periods (four days) and monitored their enantiomeric excesses. No erosion of their stereochemical composition was observed. Similarly, **3aa**-(*R*) was stirred at 30°C with **CT1**-(*S*) (1:1 ratio) to evaluate potential epimerization at carbon 4. However, after four days, no variations in *ee* was detected. This supported the contention that compounds **3** are configurationally stable at their C4 stereogenic center.

2.1 | Atropisomery Studies

^{1}H NMR analyses of the enantiomerically enriched compounds **3**, performed in various solvents (DMSO-d_6, THF-d_8, CD_3OD), revealed no evidence of rotamers at 25°C. This finding strongly

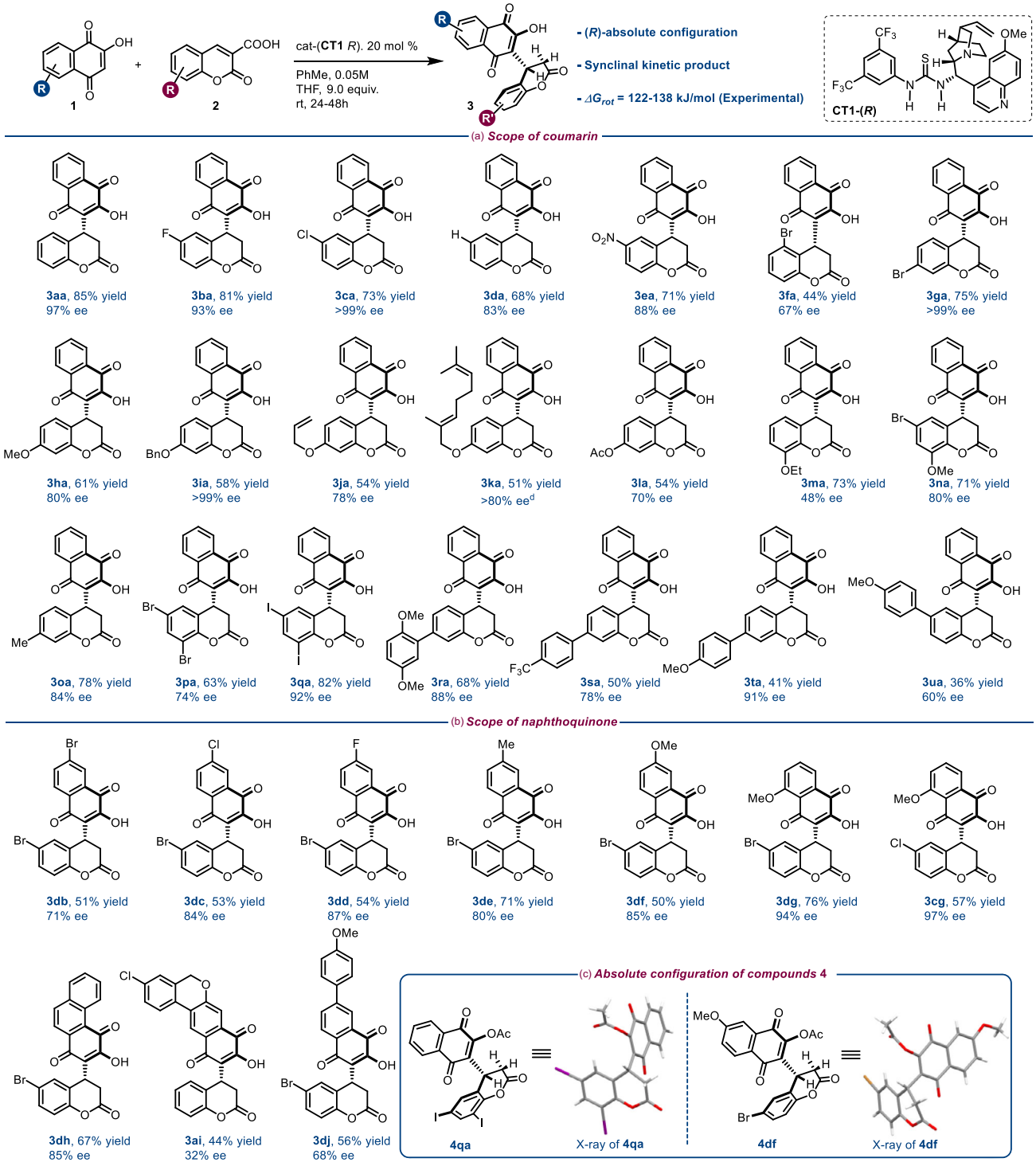

SCHEME 3 | Atroposelective 1,4 addition of naphthoquinones to coumarin-3-carboxylic acids. The experiments were conducted on a 0.2 mmol scale, in toluene (0.05 M), THF (9.0 equiv.), and **CT1** (20 mol%) at rt. The *ee* of compounds **3** was determined by chiral High Pressure Liquid Chromatography (HPLC) after acylation. (a) Substrate scope of coumarin. (b) Substrate scope of naphthoquinone. (c) X-ray diffraction analysis of compounds **4qa** (CCDC 2 465 692) and **4df** (CCDC 2 465 693). (d) The *ee* of compound **3ka** was evaluated to be >80% but could not be accurately determined by HPLC analysis owing to side-chain isomerization, which hampered chromatographic separation.

suggested that a single atropisomer might be selectively generated during the 1,4-addition reactions of naphthoquinones **2** to coumarins **1**, and that the resulting derivatives **3** could be obtained through a highly enantio and atroposelective pathway, enabling the formation of both a new stereocenter at the C4 position of the chromanone unit and a configurationally stable and well-defined C(sp^2)–C(sp^3) axis. Single-crystal X-ray diffraction of compounds **4qa** and **4df** (Scheme 3c) revealed that **4qa** crystallizes in the monoclinic C2 space group with one molecule in the asymmetric unit, whereas **4df** crystallizes in the

orthorhombic $P2_12_12_1$ space group with two independent molecules in the asymmetric unit (Figures S13–S16, Tables S9–S13). Notably, the dihedral angle (θ) between the planes formed by the naphthoquinone and chroman-2-one moieties is approximately 75° for compound **4qa**, while for the two independent molecules of compound **4df**, the angles are 85° and 87°, respectively. This suggests a synclinal (*sc*) conformation in the solid state for both cases [58]. Additionally, Nuclear Overhauser Effect Spectroscopy (NOESY) experiments conducted in solution (DMSO-d_6) with a panel of derivatives **3** indicate that these compounds consistently adopt this spatial arrangement. The rotational barriers (*sc*→*ap*→*ac*→sp) for these compounds were predicted using quantum mechanical calculations [59] showing values of approximately 136 kJ/mol for *sc* →*ac* rotations and a second higher rotational barrier of approximately 154 kJ/mol, corresponding to the interconversion sp →*ap* (Scheme 4a,b, see also SI—Section S6 and S10). This suggested that derivatives **3** likely possess high conformational stability associated with their $C(sp^2)$–$C(sp^3)$ axis

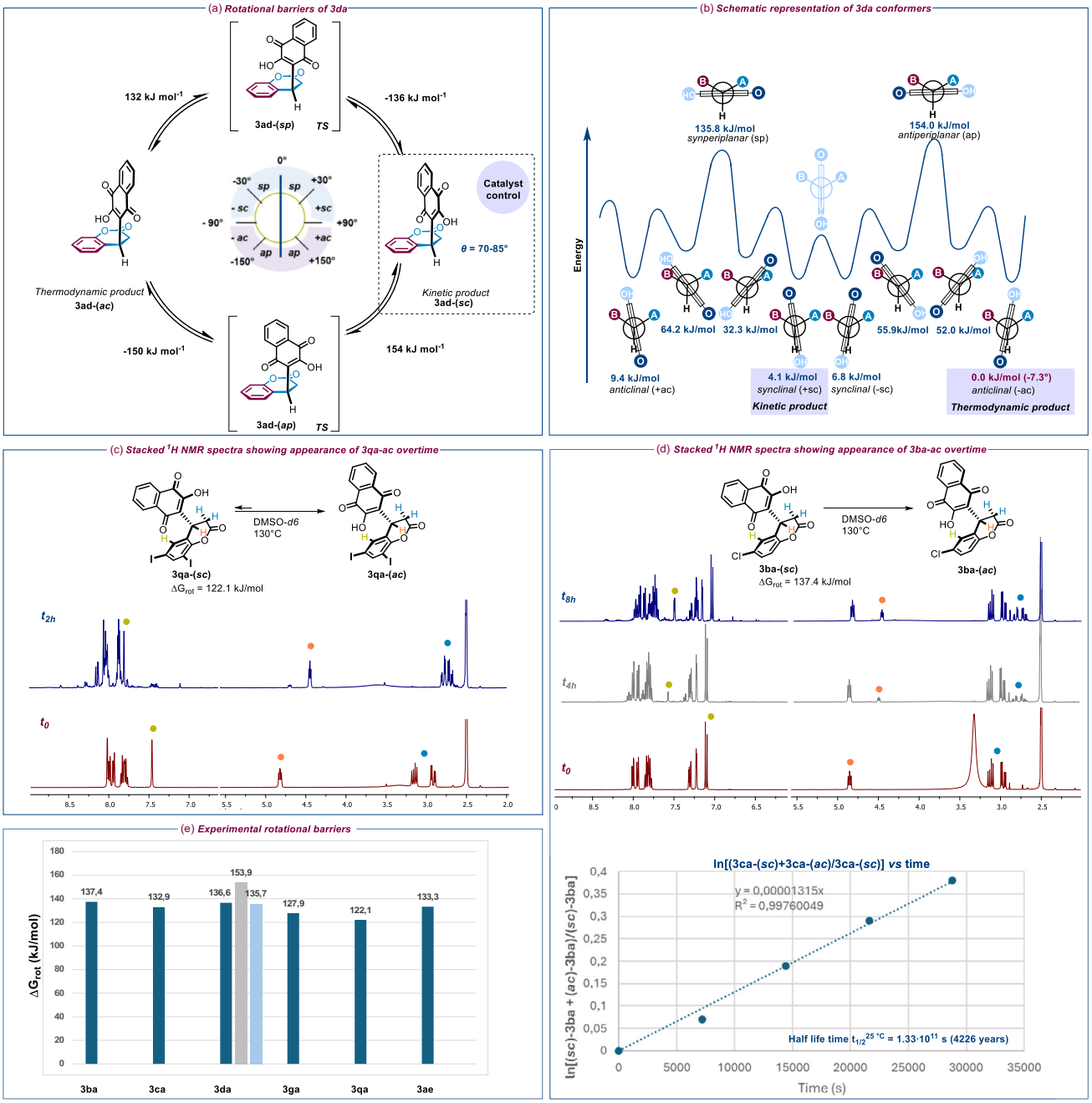

SCHEME 4 | Experimental Studies and Prediction of Rotational Barriers of Compounds **3**: NMR Evidence of synclinal-to-anticlinal conversion. (a) Rotational barriers of the **3aa** conformers. (b) Schematic attribution of the synclinal conformation to compound **3aa**-(*R*). To designate the sc and ac descriptors, the priority was assigned to the carbons next to the one bearing the stereogenic axis following Cahn-Ingold-Prelog rules, considering the aromatic C5 of the chromanone and the carbonyl group of the naphthoquinone as the two groups with the highest priority. (c) Experimental and predicted K_{rot} and ΔG_{rot} values of a panel of compounds **3**. (d) Stacked ^{1}H NMR spectra showing appearance of **3qa**-(*ac*) overtime (relevant regions); (e) Stacked ^{1}H NMR spectra showing appearance of **3ca**-(*ac*) overtime (relevant regions). For complete analyses, refer to Supporting Information—Section S6).

(see SI, sections S6 and S10) and room-temperature half-lives in the order of hundreds of years (half-life time $t_{1/2}$ (25°C) = 2.56 x 10^{10} s, i.e., 500–5000 years) [26].

To verify these data, we carried out a series of VT-NMR (Variable Temperature NMR) experiments, following procedures previously reported in the literature [26, 29]. Specifically, DMSO-d_6 solutions (0.05 M) of synclinal compounds **3aa**-**3ca**, **3ga**, **3qa**, and **3de** were heated to 130°C for several hours (2–8 h) to promote *sc*→*ac* thermal isomerization, allowing us to determine their configurational stability and the corresponding rotational barriers around their C(sp^2)–C(sp^3) axis (Scheme 4e, see also SI—Section S6). To mention some relevant examples, VT-NMR analyses for the compound 6,8-diiodo chromanone compound **3qa**-(*sc*) (*ee*: 92%, Scheme 4c) showed that the kinetic *sc*-atropisomer disappeared after 2hr heating (K_{rot} = 1.28 x 10^{-3} s^{-1} and ΔG_{rot} = 122,08 kJ/mol), leading to the formation of *a* > 99:<1 mixture of the predominant thermodynamic product **3qa**-(*ac*) resulting stable over time (half-life time $t_{1/2}$ (130°C) = 541 sec or 0.17 h, half-life time $t_{1/2}$ (60°C) = 1.38 x 10^6 s or 382 h, and half-life time $t_{1/2}$ (25°C) = 2.72 x 10^8 s or 8.6 years). The complete *sc*→*ac* interconversion was also confirmed by NOESY experiments (SI). The derivative **3qa**-(*ac*) was finally purified by flash chromatography and characterized via ^{1}H and ^{13}C NMR. Chiral High Pressure Liquid Chromatograpy (HPLC) analysis of the acetate derivative **4qa**-(*ac*) confirmed that no racemization at the chromanone C4 position occurred during the heating process and the measured *ee* remained unchanged (*ee* 91%). On the other hand, the 6-chloro chromanone **3ca**-(*sc*) showed higher stability (K_{rot} = 1.32 x 10^{-5} s^{-1} and ΔG_{rot} = 137.43 kJ/mol), requiring longer heating times and after 8h only the 32% of **3ca**-(*ac*) was formed, as shown in Scheme 4d (half-life time $t_{1/2}$ (130°C) = 5.27 x 10^4 s or 14.6 h, half-life time $t_{1/2}$ (60°C) = 3.52 x 10^8 s or 11.16 years, and half-life time $t_{1/2}$ (25°C) = 1.33 x 10^{11} s or 4226 years).

Moreover, the compound **3aa**-(*sc*), which lacks substituents that could increase steric hindrance and thereby promote rotation around the C(sp^2)–C(sp^3) axis, nevertheless exhibits high conformational stability. This unexpected rigidity can be justified by the high experimentally determined rotational barrier values (see Scheme 4e, Rotational barrier diagram), which effectively prevent axis inversion and ensure the persistence of a well-defined atropisomer even in the absence of steric reinforcement. (K_{rot} = 1.70 x 10^{-5} $s^{-1}$and ΔG_{rot} = 136.5 kJ/mol). As a matter of fact, VT-NMR analyses for **3aa**-(*sc*) revealed that only 38% was converted into the corresponding thermodynamic (*ac*)-conformer after 8 h of heating at 130°C (half-life time $t_{1/2}$ (130°C) = 4.08 x 10^4 s or 11.3 h, half-life time $t_{1/2}$ (60°C) = 2.59 x 10^8 s or 8.2 years; and, half-life time $t_{1/2}$ (25°C) = 9.40 x 10^{10} s or 2982 years). Experiments related to other compounds of this series have been summarized in the histogram included in the Scheme 5c and reported in detail in the SI, Section S6.

2.2 | Computational and Reaction Mechanism Studies

Having established the configurational stability and stereochemical robustness of derivatives **3**, we proceeded to investigate the reaction mechanism governing the atroposelective synthesis of conformationally stable C(sp^2)–C(sp^3) adducts via the tandem 1,4-nucleophilic addition/decarboxylation strategy. As reported previously, NMR titration of the catalyst **CT1**-(*R*) with increasing amounts of 2-hydroxynaphthoquinone **2a** reveals that both thiourea protons engage in hydrogen bonding (calcd. 2.0 and 2.6 Å) with the carbonyl group at position 1 of the 2-hydroxynaphthoquinone [60]. These interactions are associated with distinct downfield shifts for both protons (6.1→6.4 ppm and 8.1→8.6 ppm) as highlighted in Figures S7,S8, and Table S7. Simultaneously, density functional theory (DFT) calculations [61–64] suggested that the quinuclidine moiety of the catalyst is positioned favorably to interact with the proton of the hydroxyl group at position 2, thereby facilitating its deprotonation (Scheme 5, I). Experimental measurement of the *pKa* values for **2a** (*pKa* = 4.5 in water) and for **1a** (*pKa* = 5.0 in water) led to the conclusion that **2a** is indeed a stronger acid than **1a**, so its deprotonation may occur more rapidly than that of the coumarin 3-carboxylic acid. This deprotonation would result in an increased electron density at position 3 of the naphthoquinone, as evidenced by a chemical shift in the proton bound to carbon 3 of **2a** (7.3→7.5 ppm). The enhanced nucleophilicity at this site should enable reaction with the coumarin substrate along a well-defined trajectory, potentially stabilized by π–π interactions between the aromatic systems of the coumarin and the catalyst, as suggested by the DFT calculations (Scheme 5, II). The 1,4-nucleophilic attack on the coumarin double bond by the naphthoquinone-catalyst adduct is therefore stereochemically decisive for both the formation of the stereocenter at C4 and the establishment of the C(sp^2)–C(sp^3) axis in a synclinal spatial arrangement. This process is likely facilitated by a hydrogen-bonding network involving the enolate/enol form of the coumarin lactone and the carboxylic acid group, as also shown for the Transition State (**Ts**). Subsequent thermodynamically favored decarboxylation at position 3 (ΔH = 7.45 kJ/mol) with the loss of CO_2 (**Ts→III**) and concomitant protonation, which facilitates the formation of the **3aa**–**CT1** adduct **III** (see also scheme S1 in Supporting Information). The results of quantum mechanical predictions for this species are in strong agreement with the previously-reported findings, particularly concerning the high affinity of derivative **3** for the catalyst (**3aa**, K_{ass} = 1.03 x 10^4 M^{-1}). The energy associated with the displacement of **3aa** is higher than that of **III** but significantly lower than that of **I** (ΔH **I–III** = 9.0 kJ/mol), suggesting the need for a hydrogen-bond breaking agent by competing for the thiourea unit of **CT1**. THF plays the role of this agent (**IV**): the catalytic cycle begins and ends with CT1+THF. The reaction path is illustrated in Scheme 5 in vacuo (black), in pure toluene (pistachio) and pure THF (magenta) solvents, and in mixed toluene/THF (7.5% THF) (blue). Solvated energy levels, presented relative to gas-phase reactants, were evaluated via the COnductor-like Screening MOdel method, representing solvents as a dielectric continuum surrounding the molecules, using dielectric constants 2.3741 and 7.4257 for pure toluene and THF, respectively, and 2.4851 for toluene-THF (7.5%) evaluated from pure solvents by a Clausius-Mossotti [65–67] mixing formula. CO_2 was treated as liberated from solution and calculated in gas phase. Solvated energies are always lower than gas-phase energies and lower in THF than in toluene. To aid comparison, toluene-THF (7.5%) solvent with explicit THF bound to **CT1** is set as the zero energy reference in Scheme 5. The isolated **CT1** molecule is stabilized by THF-H bonding (2.16 and 1.91 Å, Scheme 5ii). The strength of the THF-**CT1** interaction (H-bond, together with van der Waals interactions) varies with the solvent, with binding energy of

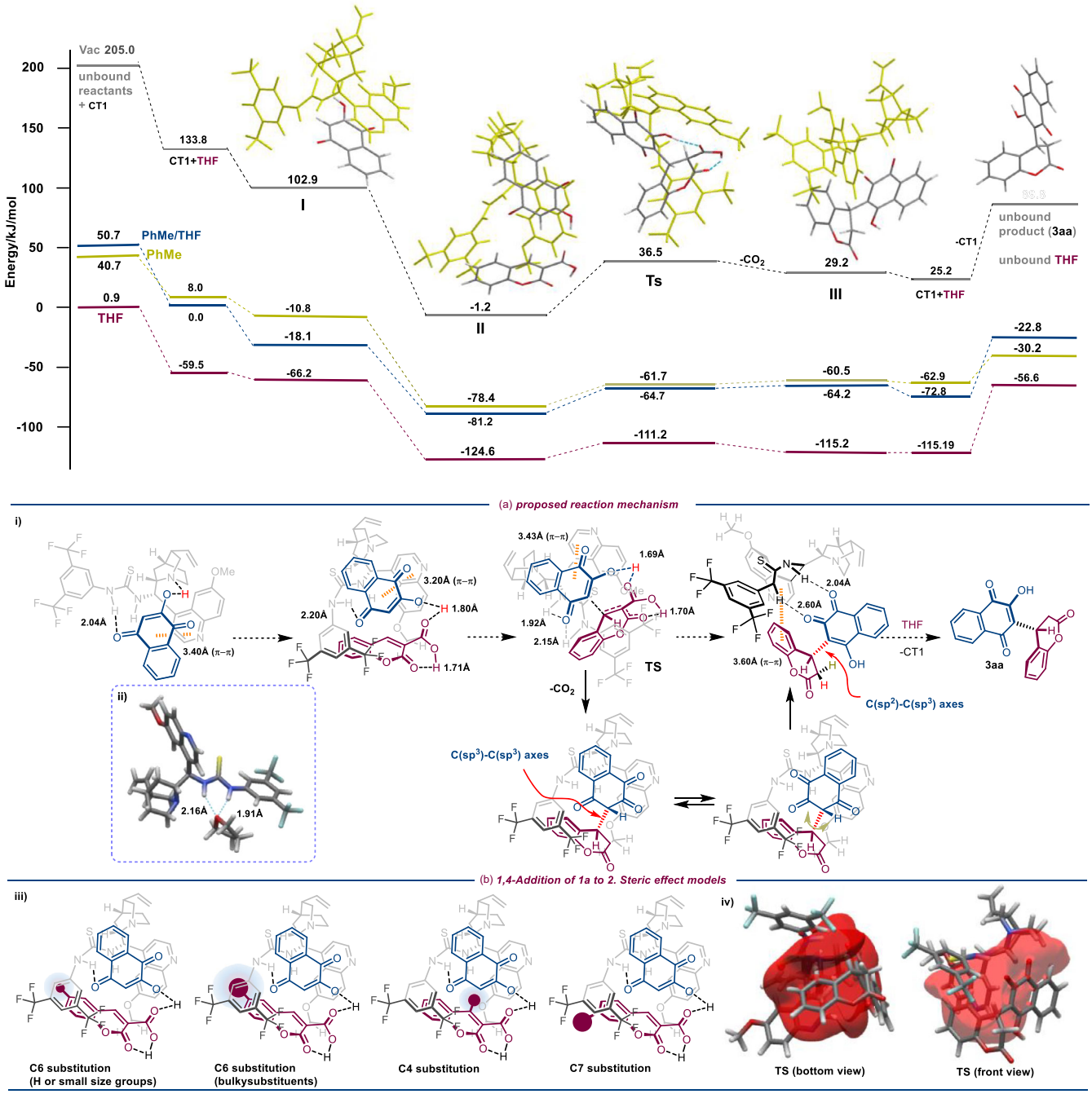

SCHEME 5 | Free-energy profile leading to products **3aa**-(*sc*). Calculations of reaction species were conducted using Kohn–Sham DFT implemented by NWChem. A B3LYP exchange-correlation functional was employed with Grimme's DFT-D3 dispersion correction using the Def2-TZVP basis set. Proposed reaction mechanism including predicted hydrogen-bonding interactions. Independent Gradient Model (IGM) steric effect models.

−71 kJ/mol in vacuum, weakening to −33 kJ/mol in pure toluene, −59 kJ/mol in pure THF solvent, and -51 kJ/mol in toluene-THF (7.5%). The catalytic reaction path proceeds via displacement of the bound THF molecule by derivative **2**, ending with liberation of the final derivative **3** via rebinding THF to **CT1** (**IV**). The change in enthalpy-liberating derivative **3** is found to be strongest in 7.5% THF with a value of −8.9 kJ/mol, compared to −3.9, −2.4, and 0 kJ/mol in vacuum and pure toluene and THF solvent, respectively. In summary, the driving force for the catalytic behavior lies in the trend that reactant (naphthoquinone **2**) binding to **CT1** is enthalpically favored relative to THF binding, while THF binding to **CT1** is enthalpically favored relative to product binding, with liberation of **3** allowing the catalytic reaction cycle to continue. On the basis of these observations and the experimental results obtained, a reaction mechanism that accounts for the formation of a hydrogen-bonding network between the reactants and the catalyst, as well as the role of THF as a promoter of catalyst turnover, is proposed in Scheme 5i.

Finally, in order to rationalize the variability in enantiomeric excess observed during the generalization of this process (Scheme 3), we further analyzed the previously computed DFT **TS** by examining the gradient of the electron density. In

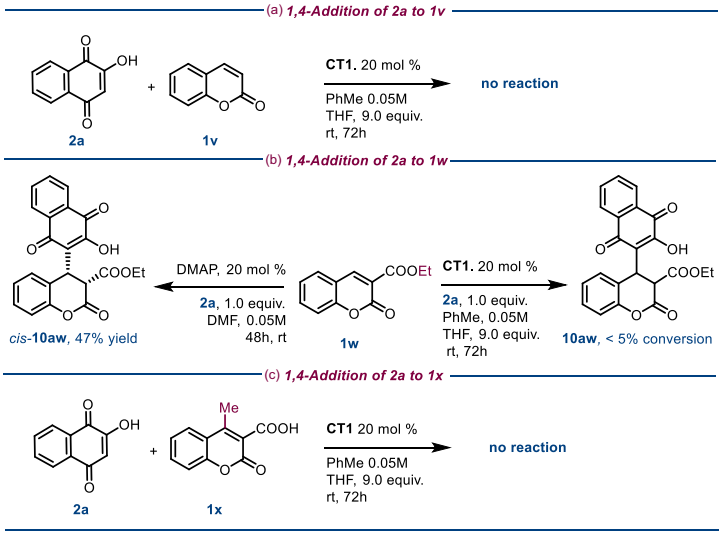

SCHEME 6 | Reactivity experiments. Unless otherwise stated, experiments were carried out using 0.2 mmol of compounds **1** and **2**, in toluene (0.05 M), THF (7.5%, 9.0 equiv.), and **CT1** as a catalyst (20 mol %) at room temperature.

particular, we employed IGM maps [68, 69], which allow the identification of regions of space where chemical interactions take place. In this case, the IGM-og analysis reveals strongly repulsive regions (highlighted in red), enabling the development of a qualitative model (Scheme 5iv, see also SI). This model delineates spatial regions where structural modifications can be introduced without perturbing the transition-state geometry, as well as areas that are not amenable to substitutions unless key intermolecular interactions are disrupted. This analysis can be used to explain why small substituents directly attached at the C6 position of the coumarin core are well tolerated (see Scheme 3, such as entries **3aa**-**3ca**), whereas increasing steric bulk and structural complexity lead to deviation from the optimal transition-state geometry (Scheme 5iii). Such distortion can disrupt the hydrogen-bonding network and other noncovalent interactions that are essential for high enantioselectivity. In particular, the introduction of bulky substituents at C6 can displace the 3,5-bis(trifluoromethyl)aryl unit of **CT1** in the **TS,** thereby weakening the interaction between the thiourea moiety and naphthoquinone **2** (Scheme 5i). Moreover, the model suggests that substituents at the C4 position other than hydrogen are not tolerated. Conversely, it supports the experimental outcomes obtained with 7-substituted coumarins, which are oriented outward from the **CT1**–coumarin–naphthoquinone supramolecular assembly without perturbing the key noncovalent interactions, thus generally affording high and remarkably uniform enantiomeric excesses.

To validate these predictions and assess the reliability of the computational model against experimental data, we conducted the experiments summarized in Scheme 6. The absence of the carboxyl group completely suppressed the formation of the 1,4-addition products, likely due to decreased electrophile reactivity and/or the loss of the crucial hydrogen-bonding network (Scheme 6a). Nevertheless, protection of the carboxyl group as an ethyl ester (**1w**) afforded racemic (*cis*)-**5wa** in moderate yield when the reaction was carried out in the presence of 4-(dimethylamino)pyridine in DMF. In contrast, reaction of **1w** with **2a** in the presence of **CT1** (20 mol %) led to the formation of **5wa** only in trace amounts (Scheme 6b). On the other hand, replacement of the C4 hydrogen with a methyl group in carboxylated coumarin derivative **1x** completely inhibited the 1,4-addition process (Scheme 6c), a result that can be attributed to the increased steric congestion at the reactive site, in full agreement with the proposed transition-state model reported in Scheme 5.

3 | Conclusions

In conclusion, we have demonstrated the feasibility of accessing a new class of naphthocoumarin derivatives through a highly enantio- and atroposelective organocatalytic approach. This process affords synclinal adducts featuring a $C(sp^2)$–$C(sp^3)$ axis with high configurational stability and rotational barriers exceeding 135 kJ/mol. Their structures were unambiguously determined by NMR and X-ray crystallographic analyses. Conformational stability studies revealed that, upon prolonged heating at 130°C, these compounds undergo conversion to the corresponding anticlinal isomers. At room temperature, the latter exhibits configurational stability in the order of decades to thousands of years ($t_{1/2}$ at 25°C > 103 years). Mechanistic investigations suggest that access to the synclinal atropisomers relies on the formation of a chiral network established through strong interactions between the reagents and the catalyst. The catalytic cycle was further optimized by the involvement of a hydrogen-bond-breaking agent (THF), which facilitated product release and enhanced catalyst turnover, thereby improving yields without affecting the enantiomeric excesses. Overall, these findings provide new perspectives for the development of catalytic strategies aimed at the synthesis of complex organic molecules with defined stereochemical features and potential pharmaceutical applications.

Acknowledgments

FSC 2020-Piano Stralcio (Fondo per lo Sviluppo e la Coesione-DOT1304455) is gratefully acknowledged for financing M. C. Cabua's PhD grant. The authors acknowledge the University Research Services Centre (CeSAR)-UniCA for technical support with particular reference to the mass-spectrometry analysis, and NMR service. A. Carlone

acknowledges funding by the European Union-Next Generation EU under the Italian Ministry of University and Research (MUR) National Innovation Ecosystem grant ECS00000041 - VITALITY - CUP E13C22001060006. A. Carlone, R. Luisi and F. Secci acknowledge financial support by the European Union Next Generation EU (PRIN 2022 PNRR - Project P2022YM7F2). D. Parsons acknowledges the support of CINECA under the ISCRA initiative, for the availability of high-performance computing resources and support.

Open access publishing facilitated by Universita degli Studi di Cagliari, as part of the Wiley - CRUI-CARE agreement.

Funding

This study was supported by Ministero dell'Università e della Ricerca (ECS00000041, MUR, P2022YM7F2).

Conflicts of Interest

The authors declare no conflicts of interest.

Data Availability Statement

The data that supports the findings of this study are available in the supplementary material of this article.

References

1. D. Lotter, A. Castrogiovanni, M. Neuburger, and C. Sparr, "Catalyst-Controlled Stereodivergent Synthesis of Atropiso-Meric Multiaxis Systems," *ACS Central Science* 4 (2018): 656–660.

2. X. Wu, R. M. Witzig, R. Beaud, C. Fischer, D. Häussinger, and C. Sparr, "Catalyst Control Over Sixfold Stereogenicity," *Nature Catalysis* 4 (2021): 457–462.

3. J. L. Gustafson, D. Lim, and S. J. Miller, "Dynamic Kinetic Resolution of Biaryl Atropisomers via Peptide-Catalyzed Asym-Metric Bromination," *Science* 328 (2010): 1251–1255.

4. I. Maclean, E. Gallent, O. Orozco, et al., "Atroposelective Synthesis of Axially Chiral Naphthylpyrroles by a Catalytic Asymmetric 1,3-Dipolar Cycloaddition/Aromatization Sequence," *Organic Letters* 26 (2024): 922–927.

5. P.-F. Wang, Y. Z.-H., S.-Y. Zhang, A. Duan, and H.-Y. Bai, "Enantioselective Synthesis of Axially Chiral Sulfone-Containing Styrenes Based on Ion-Exchange Strategy," *Organic Letters* 26 (2024): 3498–3502.

6. Q.-Z. Li, P.-F. Lian, F.-X. Tan, et al., "Organocatalytic Enantioselective Construction of Heterocycle-Substituted Styrenes with Chiral Atropisomerism," *Organic Letters* 22 (2020): 2448–2453.

7. T.-Z. Li, C.-C. Tian, W. Chen, et al., "Photoredox/Nickel-Cocatalyzed Asymmetric C-O and C-S Couplings for Atroposelective Synthesis of N-Heterobiaryls," *Angewandte Chemie International Edition* 64 (2025): e202516584.

8. D. R. Hirsch, A. J. Metrano, E. A. Stone, G. Storch, S. J. Miller, and R. P. Murelli, "Troponoid Atropisomerism: Studies on the Configurational Stability of Tropone-Amide Chiral Axes," *Organic Letters* 21 (2019): 2412–2415.

9. J. Clayden, N. Westlund, C. S. Frampton, and M. Helliwell, "Diastereoselective Synthesis of Atropisomers Containing Two Non-Biaryl Stereogenic Axes: Stereochemical Relay Through Stereogenic Centres in Dihydrostilbene-2,2′-Dicarboxamides," *Organic & Biomolecular Chemistry* 4 (2006): 455–461.

10. Y. Wei, F. Sun, G. Li, S. Y. Xu, M. X. Zhang, and L. Hong, "Enantioselective Synthesis of N–N Amide–Pyrrole Atropisomers via Paal–Knorr Reaction," *Organic Letters* 26 (2024): 2343–2348.

11. J. G. Mei, W. L. Koay, C. Y. Guan, and Y. Lu, "Atropisomers beyond the C–C Axial Chirality: Advances in Catalytic Asymmetric Synthesis," *Chem* 8 (2022): 1855–1893.

12. A. Link and C. Sparr, "Organocatalytic Atroposelective Aldol Condensation: Synthesis of Axially Chiral Biaryls by Arene Formation," *Angewandte Chemie International Edition* 53 (2014): 5458–5461.

13. Q. Shi, F. Fang, and D-J. Cheng, "Organocatalytic Atroposelective Dynamic Kinetic Resolution Involving Ring Manipulations," *Advanced Synthesis & Catalysis* 366 (2024): 1269–1284.

14. O. F. B. Watts, J. Berreur, B. S. L. Collins, and J. Clayden, "Biocatalytic En-Antioselective Synthesis of Atropisomers," *Accounts of Chemical Research* 55 (2022): 3362–3375.

15. P. Zhang, B. Yuan, J. Li, et al., "Biocatalytic Desymmetrization for the Atroposelective Synthesis of Axially Chiral Biaryls Using an Engineered Imine Reductase," *Angewandte Chemie International Edition* 137 (2025): e202416569.

16. G. Yang, S. Sun, Z. Li, Y. Liu, and J. Wang, "Organocatalytic Atroposelective Heterocycloaddition to Access Axially Chiral 2-Arylquinolines," *Communications Chemistry* 4 (2021): 1–8.

17. W. Z. Li, C.-J. Lu, J. Feng, and R. R. Liu, "Atroposelective Synthesis of C–N Vinylindole Atropisomers by Palladium-Cata-Lyzed Asymmetric Hydroarylation of 1-Alkynylindoles," *Angewandte Chemie International Edition* 62 (2023): e202312930.

18. S. Zhang, Q.-J. Yao, G. Liao, et al., "Enantioselective Synthesis of Atropisomers Featuring Pentatomic Heteroaromatics by Pd-Catalyzed C–H Alkynylation," *ACS Catalysis* 9 (2019): 1956–1961.

19. S. Cen, M. X. Zhao, N. Huang, D. Lian, A. Shen, and Z. Zhang, "Conformational Enantiodiscrimination for Asymmetric Construction of Atropisomers," *Nature Communications* 13 (2022): 4735–4742.

20. M. Nakamura and M. Oki, "Restricted Rotation Involving the Tetrahedral Carbon. 10,10-Dibenzyl-9-Aryl-10,10-Dihy-Droanthracen-9-Ols: A New System Which Exhibits a High Barrier to Rotation About A $C(sp^3)$-$C(sp^2)$ Bond," *Tetrahedron Letters* 20 (1979): 527–530.

21. K. Damodaran, S. D. Nielsen, S. J. Geib, W. Zhang, Y. Lu, and D. P. Curran, "Aryl-Csp3 Bond Rotation Barriers of 2-Aryl Perhydropyrrolo-[3,4-c]pyrrole-1,3-Diones," *Journal of Organic Chemistry* 74 (2009): 5481–5485.

22. C. Jaime, M. Rubiralta, M. Feliz, and E. Giralt, "Molecular Mechanics Calculations on the Csp3-Csp2 Rotation in the N,3,3-Trimethyl-2-Phenyl-4-Piperidone System," *Journal of Organic Chemistry* 51 (1986): 3951–3955.

23. Z. Dong, X. Ma, Y. Yu, X. Gu, and D. Zhao, "The Effect of Intramolecular Hydrogen Bonds on the Rotational Barriers of the Biaryl C-C Axis," *Chemistry – A European Journal* 29 (2023): e202302292.

24. G. D. Bisag, D. Pecorari, A. Mazzanti, et al., "Central-to-Axial Chirality Conversion Approach Designed on Organocatalytic Enantioselective Povarov Cycloadditions: First Access to Configurationally Stable Indole–Quinoline Atropisomers," *Chemistry – A European Journal* 25 (2019): 15694–15701.

25. N. Di Iorio, G. Filippini, A. Mazzanti, P. Righi, and G. Bencivenni, "Controlling the C(sp3)-C(sp2) Axial Conformation in the Enantioselective Friedel-Crafts-Type Alkylation of β-Naphthols with Inden-1-Ones," *Organic Letters* 19 (2017): 6692–6695.

26. G. Bertuzzi, V. Corti, J. A. Izzo, S. Ričko, I. N. Jessen, and C. A. Jørgensen, "Organocatalytic Enantioselective Construction of Conformationally Stable C(sp2)–C(sp3) Atropisomers," *Journal of the American Chemical Society* 144 (2022): 1056–1065.

27. J. K. Cheng, S.-H. Xiang, S. Li, L. Ye, and B. Tan, "Recent Advances in Catalytic Asymmetric Construction of Atropisomers," *Chemical Reviews* 121 (2021): 4805–4902.

28. N. Tampellini, P. Righi, and G. Bencivenni, "Computational Investigation on the Origin of Atroposelectivity for the Cinchona

Alkaloid Primary Amine-Catalyzed Vinylogous," *Journal of Organic Chemistry* 86 (2021): 11782–11793.

29. A. Domain, G. Bai, J. C. Castillo, et al., "Stereocontrol in Conformationally Stable $C(sp^2)$–$C(sp^3)$ Atropisomers," *Angewandte Chemie International Edition* 64 (2025): e202506810.

30. S. Perreault, J. Chandrasekhar, and L. Patel, "Atropisomerism in Drug Discovery: A Medicinal Chemistry Perspective Inspired by Atropisomeric Class I PI3K Inhibitors," *Accounts of Chemical Research* 55 (2022): 12581–2593.

31. M. Basilaia, M. H. Chen, J. Secka, and J. L. Gustafson, "Atropisomerism in the Pharmaceutically Relevant Realm," *Accounts of Chemical Research* 55 (2022): 2904–2919.

32. T. Yao, C. Yuan, X. Wang, H. Zhai, and C. Zhao, "Organocatalytic Enantio-, Atrop-, and Diastereoselective Macrocyclization of Quinone Methides," *CCS Chemistry*. (2025): 1–10.

33. M. Bouda, G. E. Hana, D. Xhili, A. Sripada, J. A. Bertke, and C. Wolf, "Organocatalytic Atroposelective Fluorooxindole Addition to Coumarin Michael Acceptors," *Chemical Communications* 61 (2025): 7883–7886.

34. A. Cocco, S. Paniziutti, C. Olla, et al., "Design, Synthesis, and Photophysical Characterization of Biocompatible Thermally Activated Delayed Fluorescent Carbazole-Coumarins for Sensing Applications," *Chemistry – A European Journal* 30 (2024): e202401263.

35. A. Cocco, P. Caria, G. Sanna, et al., "Synthesis and Photophysical Properties of Fluorescent 6-Aryl-D-π-A Coumarin Derivatives," *ACS Omega* 6 (2021): 33708–33716.

36. A. Luridiana, G. L. Pretta, D. Chiriu, et al., "A Facile Strategy for New Organic White LED Hybrid Devices: Design, Features and Engineering," *RSC Advances* 6 (2016): 22111–22120.

37. A. Luridiana, A. Frongia, D. J. Aitken, R. Guillot, G. Sarais, and F. Secci, "Deracemizing Organocatalyzed Michael Addition Reactions of 2-(Arylthio)Cyclobutanones with β-Nitrostyrenes," *Organic & Biomolecular Chemistry* 14 (2016): 3394–3403.

38. F. Capitta, A. Frongia, J. Ollivier, et al., "Enantioselective Organocatalyzed Desymmetrization of 3-Substituted Cyclobutanones through Michael Addition to Nitroalkenes," *Synlett* 26 (2015): 123–126.

39. Z. Shao, L. Xu, L. Wang, H. Wei, and J. Xiao, "Catalyst-Free Tandem Michael Addition/Decarboxylation of (Thio)Coumarin-3-Carboxylic Acids with Indoles: Facile Synthesis of Indole-3-Substituted 3,4-Dihydro(Thio)Coumarins," *Organic & Biomolecular Chemistry* 12 (2014): 2185–2188.

40. B. Kumar, B. Borah, J. N. Babu, and L. R. Chowhan, "Direct Michael Addition/Decarboxylation Reaction Catalyzed by a Composite of Copper Ferrite Nanoparticles Immobilized on Microcrystalline Cellulose: An Eco-Friendly Approach for Constructing 3,4-Dihydrocoumarin Frame-Works," *RSC Advances* 12 (2022): 30704–30711.

41. S. Peng, L. Wang, H. Guo, S. Sun, and J. Wang, "Facile Synthesis of 4-Substituted 3,4-Dihydrocoumarins via an Organocatalytic Double Decarboxylation Process," *Organic & Biomolecular Chemistry* 10 (2012): 2537–2541.

42. E. Kowalska, A. Artelska, and A. Albrecht, "Visible Light-Driven Reductive Azaarylation of Coumarin-3-Carboxylic Acids," *The Journal of Organic Chemistry* 87 (2022): 9645–9653.

43. S. Nakamura, A. Toda, M. Sano, T. Hatanaka, and Y. Funahashi, "Organocatalytic Enantioselective Conjugate Addition of Malonic Acid Half Thioesters to Coumarin-3-Carboxylic Acids Using N-Heteroarenesulfonyl Cinchona Alkaloid Amides," *Advanced Synthesis & Catalysis* 358 (2016): 1029–1034.

44. F. Hueso-Idaira, A. Amesty, L. Anaissi-Afonso, A. Lorenzo-Castrillejo, F. Machín, and A. Estévez-Braun, "Synthesis and Biological Evaluation of Naphthoquinone-Coumarin Conjugates as Topoisomerase II Inhibitors," *Bioorganic & Medicinal Chemistry Letters* 27 (2017): 484–489.

45. Q. Gong, J. Hu, P. Wang, X. Li, and X. Zhang, "A Comprehensive Review on β-Lapachone: Mechanisms, Structural Modifications, and Therapeutic Potentials," *European Journal of Medicinal Chemistry* 210 (2021): 112962–112949.

46. T. Ishikawa, K. I. Kotake, and H. Ishii, "Synthesis of Toddacoumaquinone, a Coumarin-Naphthoquinone Dimer, and Its Antiviral Activities," *Chemical and Pharmaceutical Bulletin* 43 (1995): 1039–1041.

47. R. Sagar, U. Shankar, A. Khanna, K. Singh, and G. Tiwari, "Recent Advances in the Synthesis of 2-Hydroxy-1,4-Naphthoquinone (Lawsone) Derivatives," *SynOpen* 7 (2023): 619–651.

48. C. Qi, W. Wang, K. D. Reichl, J. McNeely, and J. A. Porco, "Total Synthesis of Aurofusarin: Studies on the Atropisomeric Stability of Bis-Naphthoquinones," *Angewandte Chemie International Edition* 57 (2018): 2101–2104.

49. K. Yoshida, R. Itoyama, M. Yamahira, et al., "Synthesis, Resolution, and Biological Evaluation of Atropisomeric (a *R*)- and (a *S*)-16-Methyllamellarins N: Unique Effects of the Axial Chirality on the Selectivity of Protein Kinases Inhibition," *Journal of Medicinal Chemistry* 56 (2013): 7289–7301.

50. C. Denhez, P. Lameiras, and H. Berber, "Atropisomerism About Aryl–$C(sp^3)$ Bonds: Chemically Driven Rotational Pathway in Cannabidiol Derivatives," *Organic & Biomolecular Chemistry* 21 (2023): 9572–9582.

51. Kass values were determined using BindFit, http://supra-molecular.org.

52. P. Thordarson, "Determining Association Constants from Titration Experiments in Supramolecular Chemistry," *Chemical Society Reviews* 40 (2011): 1305–1323.

53. D. Brynn Hibbert, and P. Thordarson, "The Death of the Job Plot, Transparency, Open Science and Online Tools, Uncertainty Estimation Methods and Other Developments in Supramolecular Chemistry Data Analysis," *Chemical Communications* 52 (2016): 12792–12805.

54. D. S. Potts, D. T. Bregante, J. S. Adams, C. Torresa, and D. W. Flaherty, "Influence of Solvent Structure and Hydrogen Bonding on Catalysis at Solid–Liquid Interfaces," *Chemical Society Reviews* 50 (2021): 12308–12337.

55. K. M. Lippert, K. Hof, D. Gerbig, et al., "Hydrogen-Bonding Thiourea Organocatalysts: The Privileged 3,5-Bis(trifluoromethyl)phenyl Group," *European Journal of Organic Chemistry* 2012 (2012): 5919–5927.

56. S. Tang, N. T. Tsona, and L. Du, "Ring-Size Effects on the Stability and Spectral Shifts of Hydrogen Bonded Cyclic Ethers Complexes," *Scientific Reports* 8 (2018): 1553–1564.

57. G. Y. Han, P. F. Su, Q. Q. Pan, X.-Y. Liu, and X.-Z. Shu, "Enantio-Convergent and Regioselective Reductive Coupling of pro-Pargylic Esters with Chlorogermanes by Nickel Catalysis," *Nature Catalysis* 7 (2024): 12–20.

58. G. P. Moss, "Basic Terminology of Stereochemistry," *Pure and Applied Chemistry* 68 (1996): 2193–2222.

59. To determine a rotation energy profile around the naphthoquinone-chromanone bond of the intermediate products 3, the energy-minimized geometry was taken as 0°. The bond rotation tool in Avogadro2 was then employed to manually rotate the lower moiety around the bond. The rotation energy profiles were evaluated for a series of deriv-atives, shown in Scheme 5c (See also SI, Section 2). The barrier heights for each case are reported in Table S21. 3aa showed a theoretical barrier height of 135.8 kJ/mol, corresponding to an Eyring reaction half-life $\tau = \ln 2/ kr$ of 2159 years at 25°C, consistent with NMR measurements. Eying reaction constant was evaluated as kr =, (kT/h) exp(-ΔUbarrier/RT), where ΔUbarrier is the rotational energy barrier in kJ/mol.

60. D. N. Todkary, A. Rane, and S. P. Gejji, "Hydrogen Bonding Motif in 2-Hydroxy-1,4-Naphthoquinone," *Theoretical Chemistry Accounts* 113 (2005): 161–166.

61. Quantum chemical calculations of reaction species were conducted using Kohn-Sham Density Functional Theory (DFT) implemented by NWChem. A B3LYP exchange-correlation functional was employed with Grimme's DFT-D3 dispersion correction. The Def2-TZVP basis set was used.

62. E. Aprà, E. J. Bylaska, W. A. de Jong, et al., "NWChem: Past, Present, and Future," *Journal of Chemical Physics* 152 (2020): 178.

63. S. Grimme, J. Antony, S. Ehrlich, and H. Krieg, "A Consistent and Accurate Ab Initio Parametrization of Density Functional Dispersion Correction (DFT-D) for the 94 Elements H-Pu," *Journal of Chemical Physics* 132 (2010): 154104.

64. F. Weigend and R. Ahlrichs, "Balanced Basis Sets of Split Valence, Triple Zeta Valence and Quadruple Zeta Valence Quality for H to Rn: Design and Assessment of Accuracy," *Physical Chemistry Chemical Physics* 7 (2005): 3297–3305.

65. R. Clausius, *Die Mechanische wärmetheorie*, (Wellesley College Library, 1874), 94.

66. P. Van Rysselberghe, "Remarks Concerning the Clausius-Mussotti Law," *The Journal of Physical Chemistry A* 36 (1932): 1152–1155.

67. W. M. Robertson, G. Arjavalingam, and S. L. Shinde, "Microwave Dielectric Measurements of Zirconia-Alumina Ceramic Composites: A Test of the Clausius–Mossotti Mixture Equations," *Journal of Applied Physics* 70 (1991): 7648.

68. C. Lefebvre, J. Klein, H. Khartabil, J. C. Boisson, and E. Hénon, "IGMPlot: A Program to Identify, Characterize, and Quantify Molecular Interactions," *Journal of Computational Chemistry* 44 (2023): 1750–1766.

69. C. Lefebvre, H. Khartabil, J. C. Boisson, J. Contreras-García, J. P. Piquemal, and E. Hénon, "The Independent Gradient Model: A New Approach for Probing Strong and Weak Interactions in Molecules from Wave Function Calculations," *ChemPhysChem* 19 (2018): 724–735.

Supporting Information

Additional supporting information can be found online in the Supporting Information section. The authors have cited additional references within the Supporting Information [34–66].